Published in final edited form as:
Sci Transl Med. 2017 January 18; 9(373): . doi:10.1126/scitranslmed.aag2196.

Reporter Gene Imaging of Targeted T-Cell Immunotherapy in Recurrent Glioma

Khun Visith Keu[#1,2], **Timothy H. Witney**[#1,3], **Shahriar Yaghoubi**[#1], **Jarrett Rosenberg**[1], **Anita Kurien**[4], **Rachel Magnusson**[4], **John Williams**[5], **Frezghi Habte**[1], **Jamie R. Wagner**[6], **Stephen Forman**[6], **Christine Brown**[6], **Martin Allen-Auerbach**[5], **Johannes Czernin**[5], **Winson Tang**[7], **Michael C. Jensen**[8], **Behnam Badie**[4], and **Sanjiv S. Gambhir**[1,9,‡]

[1]Department of Radiology, Molecular Imaging Program, Stanford University, Palo Alto, CA, 94305, United States

[2]Division of Nuclear Medicine, Hôpital de la Cité-de-la-Santé de Laval, QC, H7M 3L9, Canada

[3]Centre for Advanced Biomedical Imaging, Division of Medicine, University College London, London, WC1E 6DD, UK

[4]Neurosurgery, City of Hope, Duarte, CA, 91010, United States

[5]Molecular & Medical Pharmacology, UCLA, Los Angeles, CA, 90095, United States

[6]Hematology and Hematopoietic Cell Transplantation, City of Hope, Duarte, CA, 91010, United States

[7]Sangamo BioSciences Inc, Richmond, CA 94804, United States

[8]Ben Towne Center for Childhood Cancer Research, Seattle Children's Research Institute, Seattle, Washington, 98145, United States

[9]Department of Bioengineering, Department of Materials Science & Engineering, Bio-X, Stanford University, Palo Alto, CA, 94305, United States

[#] These authors contributed equally to this work.

Abstract

[‡]**Corresponding author**, Sanjiv Sam Gambhir, Stanford University School of Medicine, James H. Clark Center, 318 Campus Drive, 150 East Wing, 1st Floor, Stanford, CA 94305-5427, Tel: +01 650 725-2309, Fax: +01 650 498-5047, sgambhir@stanford.edu.

Author contributions: The project was initially conceptualized and the entire project supervised by S.S.G. The therapeutic trial leads were M.C.J., B.B., and C.B. The imaging study was designed by S.S.G. and S.Y. Image/data acquisition was performed by K.V.K., S.Y., A.K., R.M., J.W., J.R.W., S.F., C.B., M.A., J.C., W.T., T.H.W., J.R., M.C.J., B.B., and S.S.G. K.V.K., T.H.W., S.Y., F.H. J.R., B.B. and S.S.G. participated in the design and/or interpretation of the reported experiments or results. T.H.W. and K.V.K. wrote the manuscript draft, which was then further refined by S.S.G. All other authors reviewed and edited the intermediate and final versions of the manuscript.

Competing interests: Drs. C. Brown and M. Jensen are inventors on patent application WO 02/088334 held by City of Hope National Medical Center that covers Chimeric Immunoreceptor Useful in Treating Human Cancers. Drs. Yaghoubi and Gambhir are co-founders and equity holders of CellSight Inc. that develops strategies to image cell therapies in humans. Dr. Michael Jensen is on the scientific advisory board and equity holder of Juno Therapeutics, which develops novel cancer immunotherapies.

Data and materials availability: Various reporter gene constructs and cell products are available from Dr. Sanjiv Sam Gambhir under a material agreement with Stanford University and/or the City of Hope National Medical Center.

Europe PMC Funders Author Manuscripts

High-grade gliomas are aggressive cancers that often become rapidly fatal. Immunotherapy using $CD8^+$ cytotoxic T lymphocytes (CTLs), engineered to express both herpes simplex virus type-1 thymidine kinase (HSV1-TK) and interleukin (IL)-13 zetakine chimeric antigen receptor (CAR), is a treatment strategy with considerable potential. To optimize this and related immunotherapies, it may be helpful to monitor CTL viability and trafficking to glioma cells. We show that noninvasive positron emission tomography (PET) imaging with 9-[4-[^{18}F]fluoro-3-(hydroxymethyl)butyl]guanine ([^{18}F]FHBG) can track *HSV1-tk* reporter gene expression present in CAR-engineered CTLs. [^{18}F]FHBG imaging was safe and enabled the longitudinal imaging of T cells stably transfected with a PET reporter gene in patients. Further optimization of this imaging approach for monitoring in vivo cell trafficking should greatly benefit various cell-based therapies for cancer.

Introduction

Immunotherapy holds great potential for the treatment and management of cancer patients with advanced disease (1). Through numerous divergent mechanisms, including monocyte maturation in the presence of tumor antigens (2) and the genetic engineering of immune cells (3), the body's adaptive immune system can be primed to target malignancies normally recognized as 'self'. Although the success of recent Phase III trials has validated the principle that immunotherapy can sometimes extend cancer patient survival (4), tumor cells can escape immune surveillance and develop resistance to immunotherapy (5). Examples of resistance mechanisms include the regulation of immune checkpoints (6), resistance to cell-death signaling (7), or regulation by other tumor-associated immune cells, such as regulatory T cell lymphocytes (8). Given the variable success of immunotherapy in the clinic (9–11), there is an urgent need to design noninvasive techniques that could give early indications of response to treatment and help predict patient outcome.

Current methods used for the assessment of tumor response to therapy primarily rely on measurements of tumor size through anatomical imaging using the response evaluation criteria in solid tumors (RECIST) (12). The limitations of anatomical imaging for response monitoring in solid tumors have been well documented (13). Assessment of immunotherapy efficacy provides particular challenges in that the influx of effector cells to the tumor microenvironment may result in "pseudoprogression" as defined by RECIST, which is not linked to long-term outcome (14). These limitations have led to the development of a specific set of immune-related response criteria (irRC) (14, 15). irRC measurements, however, provide no biological information and can take between 8–12 weeks for an initial response assessment, by which time non-responding patients may have missed their therapeutic window and experienced unnecessary therapy-related toxicity. In addition, adaptive immune responses involving T and B lymphocytes, which have demonstrated great therapeutic potential, require monitoring of immune cell trafficking to the tumor site, lymphocyte retention, and immune cell engagement with the tumor cells. At present, techniques to non-invasively assess the in vivo viability and trafficking of these immune cells in cancer patients are not available.

We previously provided a demonstration of imaging cells in a single case report using reporter gene technology (16). In that case study, therapeutic T cells expressing a positron emission tomography (PET) reporter gene were injected into the tumor resection site of a 57-year old male high-grade glioma patient and then visualized by molecular imaging with a PET reporter probe (16). For that study, we used genetically modified $CD8^+$ autologous cytotoxic T lymphocytes (CTLs) stably expressing the chimeric antigen receptor (CAR) interleukin (IL)-13 zetakine for IL13Rα2+ tumor targeting (17–19) and the herpes simplex virus type-1 thymidine kinase gene (*HSV1-tk*) as a dual-purpose suicide (20, 21) and imaging reporter gene (Fig. 1) (22, 23). *HSV1-tk* was fused in-frame with the hygromycin phosphotransferase (*hph*) gene and expressed as a fusion protein. HPH expression conferred hygromycin B resistance for dominant positive selection. Through imaging of *HSV1-tk* reporter gene expression using 9-[4-[^{18}F]fluoro-3-(hydroxymethyl)butyl]guanine ([^{18}F]FHBG), which is a fluorine-18 radiolabeled analogue of the anti-herpes drug penciclovir (Fig. 1 *insert*), we were able to image [^{18}F]FHBG trapping in the brain tumor, thought to correspond to CTL accumulation. This corroborated the extensive preclinical assessment of this targeted strategy (24). This study in a single patient was limited, however, because at that time we only had FDA approval to perform one PET scan after the infusion of CTLs and did not have a critical baseline PET image before CTL injection. We were therefore unable to confirm that the brain-associated [^{18}F]FHBG signal was CTL-specific (22).

Expanding on this pilot case study, we sought to assess the ability of [^{18}F]FHBG to longitudinally monitor CTL trafficking, survival, and proliferation in multiple patients with recurrent high-grade gliomas that were resistant to conventional therapies. Under this protocol, seven patients received several infusions of either autologous or allogeneic engineered CTLs (Fig. 1). CTL location and response were noninvasively measured by PET using a strategy outlined in Fig. 2. In addition, we evaluated the safety of the CTLs injected into the central nervous system and the safety of recombinant human IL-2 delivery in conjunction with CTL adoptive cell transfer, a strategy used to prolong the survival of engineered CTLs and potentially improve their therapeutic efficacy.

Results

Patient enrolment and CTL characterization

To conduct a detailed evaluation of the utility of [^{18}F]FHBG to track genetically engineered CTLs for immunotherapy, we enrolled a total of 4 men and 3 women (average age of 57 ± 8 years old with recurrent high-grade glioma, under two separate IRB-approved protocols (Table 1). Patient 1 in this study is the patient from our previous case report (16). Autologous (NCT00730613)(17) and allogeneic (NCT01082926) CTLs for immunotherapy were engineered to express the tumor-targeting IL-13 zetakine CAR and the wild-type *HSV1-tk* gene reporter. This CAR recognizes IL13Rα2, a cell surface receptor expressed in over 50% of glioblastoma cells, but not in normal brain tissue (25, 26). The CTLs were > 99% CD8. We first confirmed our previous finding (27, 28) that [^{18}F]FHBG specifically accumulates in genetically modified CTLs expressing the *HSV1-tk* reporter gene rather than the naïve parental cells obtained from a human buffy coat (fig. S1). Here, [^{18}F]FHBG

accumulation at one hour was 12-fold higher in transfected CTLs versus non-transfected parental cells, at 7.37 ± 2.17 % [^{18}F]FHBG uptake/10^8 cells and 0.61 ± 0.27 % [^{18}F]FHBG uptake/10^8 cells, respectively (n = 3; P = 0.006). Furthermore, 60 min incubation with [^{18}F]FHBG had no significant effect on cell proliferation of non-transduced CTLs or those expressing *HSV1-tk* (taken from Patient 1), up to 48 h after addition of the radiotracer (fig. S2; P > 0.05).

Safety

[^{18}F]FHBG PET scans were performed in patients before and after CTL infusions to assess the spatial location of the engineered CTLs within the body. Patients 3-7 received IL-2 infusions to improve CTL survival. Patient vital signs and lab results were within normal limits throughout and after [^{18}F]FHBG administration. Patient 1 experienced a mild, transient headache without any neurological deficits. Patient 2 developed new neurological deficits two days before the initiation of CTL therapy, corresponding to vasogenic cerebral edema (diagnosed from MRI) and not related to either [^{18}F]FHBG or disease progression. Patient 5 had a mild rash on the shoulders with redness on the lower face at two hours after intravenous injection of [^{18}F]FHBG during pre-CTL imaging. Twenty-five milligrams of oral diphenhydramine was subsequently administered to Patient 5, and the rash resolved within one hour. None of the seven patients had any major or life-threatening events related to [^{18}F]FHBG or CTL injections throughout the duration of their participation within this trial. Most patients died within 12 months after the last CTL infusion. Patient survival data after initial diagnosis and since the first CTL infusion are presented in table S1.

Biodistribution

The stability and detailed pharmacokinetics of [^{18}F]FHBG in healthy volunteers have been previously reported (29). Here, we observed similar radiotracer biodistribution (fig. S3), as assessed by standardized uptake value $(SUV)_{mean}$ measurements on the pre- and post-CTL injection scans using a 50 mm diameter spherical volume of interest. In pre-CTL treatment scans, at a mean time of 137 ± 11 min after injection of [^{18}F]FHBG (n = 6), the average (±SD) SUV_{mean} was 0.25 ± 0.08 for left ventricular blood pool, 1.57 ± 0.69 for right hepatic dome, 0.09 ± 0.04 for lung parenchyma, and 0.36 ± 0.14 for right thigh. There was no significant difference in [^{18}F]FHBG uptake in these tissues after immunotherapy (P > 0.05; table S2). In the normal brain, contralateral to either suspected lesions or resection sites, and before CTL infusions, [^{18}F]FHBG SUV_{mean} was 0.04 ± 0.01 (n = 6). After CTL infusions, we observed no significant change in normal brain uptake (SUV_{mean} = 0.04 ± 0.01; n = 6; P > 0.05). We next quantified the amount of [^{18}F]FHBG activity in the vicinity of tumors where a breakdown of the blood-brain barrier was observed based on the post-contrast T1-weighted MRI scan. The low background from non-target tissue (normal brain) permitted visualization of brain tissue abnormalities such as tumors (Fig. 3A), with [^{18}F]FHBG uptake in untreated tumors and sites of tumor resection statistically higher than in the normal contralateral brain tissue (3.3-11.5-fold increase, P = 0.0009).

[^{18}F]FHBG imaging of CTLs in patients

Given the observation of some nonspecific [^{18}F]FHBG retention in both gliomas and previous surgical sites before CTL infusion, it was essential to perform baseline and follow-

up scans in the same patients after CTL injection (16). A total of ten tumor foci were analyzed in the seven patients, with two sites each assessed for Patients 1, 4, and 7. We did not obtain a pre-CTL [^{18}F]FHBG scan in Patient 1 because the use of two [^{18}F]FHBG scans per patient was not yet approved by the FDA when the patient was enrolled in 2006. Qualitative assessment of [^{18}F]FHBG uptake by PET imaging revealed an increase in PET signal after CTL infusions, likely corresponding with CTL cell trafficking and viability (Fig. 3A & B and movie S1).

To quantify [^{18}F]FHBG radioactivity and distribution, we initially evaluated the maximum concentration (SUV_{max}) of [^{18}F]FHBG on pre- and post-CTL injection scans, where we observed a large variation in response, ranging from +53% (Patient 2) to -15% (Patient 7, lesion B) (fig. S4). After intracerebral injection, there is potential for CTLs to diffuse in the surgical cavity or the brain parenchyma. To optimize the monitoring of CTL trafficking to targeted areas, better imaging metrics were needed to replace single-voxel measurements such as SUV_{max}, particularly when the localization of CTLs, and therefore the volume of interest (VOI), was unknown. The first challenge was to define an accurate VOI. Given the availability of contrast-enhanced MR images taken from the same patients before and after CTL infusions, it was possible to derive VOIs from enhancing regions of the tumor. MRI-based [^{18}F]FHBG voxel analysis, however, excluded radioactivity outside of enhancing regions (fig. S5A), which may represent CTLs that have failed to target to the tumor or potential targeting to tumor cells that were not visible on MRI. Analysis of these therapeutic cells is essential, because an indication of poor CTL trafficking to tumor tissue has implications for the efficacy of the immunotherapy strategy. To circumvent the exclusion of non-tumor-associated radioactivity, we used different SUV_{max} thresholds to draw a growing volume of interest. The contouring algorithm used selected the highest [^{18}F]FHBG SUV as the center of the VOI before generating peripheral limits based upon the desired threshold value, as illustrated in fig. S5B. VOIs for all patients were analyzed using threshold values from 10% to 90% in 10% increments (fig. S6). For [^{18}F]FHBG analysis, a 50% SUV_{max} threshold was selected to create VOIs that best represented [^{18}F]FHBG distribution throughout the brain.

Having determined a suitable, non-biased method for VOI delineation, the next challenge was to devise a method of analysis that could assess CTL trafficking 1) to a region within the brain of fixed volume, such as a tumor and 2) when the [^{18}F]FHBG signal was widely dispersed after CTL infusions, for example as a result of poor trafficking to the tumor site, CTL dilution in the ventricular system, or correct trafficking to tumor tissue not visible by MRI. The SUV_{mean} provided a means to assess tumor-specific CTL trafficking when the VOI did not change between pre- and post-CTL scans (fig. S7; Patients 2 and 6), but failed to accurately depict changes in [^{18}F]FHBG radioactivity after CTL infusions in patients for whom the VOI was increased in the post-CTL scan. To detect potential changes in [^{18}F]FHBG radioactivity before and after CTL infusions, regardless of the size of the VOI, we next assessed the total [^{18}F]FHBG activity (SUV_{mean} × volume of interest) for each scan.

Analysis of the total activity in patients for whom the size of the VOI did not change, such as Patient 6, clearly indicated a shift in SUV histograms after CTL infusions (Fig. 3C), corresponding to a doubling of total [^{18}F]FHBG activity from 4.1 to 8.4 in this patient. A

further example is provided with Patient 2, whose total activity was increased from 10.1 to 20.3 (fig. S8). Total activity measurements were also able to detect radioactivity disseminated over an increased volume after CTL infusions, an example of which is illustrated in Fig. 4A,B (Patient 7). Here, as evident from histogram analysis (Fig. 4C), despite an absence of a large change in median [^{18}F]FHBG radioactivity between scans, the total radioactivity increased 3.7-fold, from 1.8 in the pre-CTL scan to 6.8 post-CTL infusions, in part because of a substantial increase in the VOI. A further example of changes in [^{18}F]FHBG total activity after CTL infusions in the absence of a change in SUV_{mean} was observed with Patient 3 (fig. S9). Across all patients, in clinically-confirmed sites of tumor recurrence, [^{18}F]FHBG total activity was significantly increased in the PET scan after CTL infusions versus the baseline scan (Fig. 5; $P = 0.014$; paired Wilcoxon test).

[^{18}F]FHBG uptake in untreated tumor sites

In patients with multifocal disease, in addition to the injected tumor site, distant tumor foci not injected with CTLs were also analyzed with [^{18}F]FHBG (Patient 7; Fig. 4D-F). No CTLs were infused locally, and therefore no changes in [^{18}F]FHBG uptake at the site were expected between scans. In the post-CTL scan, however, a 66% increase in total [^{18}F]FHBG activity was measured by comparison to the baseline scan, from 1.6 to 2.7, further supported by minimal changes in the dispersion of voxel intensities (Fig. 4F). This is in contrast to the 5-15-fold changes observed at the injected disease site (Fig. 5). Small changes in [^{18}F]FHBG uptake at untreated tumor sites after CTL versus baseline scans were confirmed in an additional patient (Patient 4). In this patient, [^{18}F]FHBG total activity in the CTL-treated focus was increased 2.2-fold on the post-CTL scan, increasing from 2.9 at baseline to 6.3 at the site of tumor recurrence, whereas the focus corresponding to the primary untreated site increased just 32%, from 2.4 to 3.2 (fig. S10). The modest increase in [^{18}F]FHBG activity in the untreated sites in these two patients may represent trafficking of CTLs to distant tumor foci in the brain.

Challenges of CTL tracking with [^{18}F]FHBG

As a result of the complexity of implementing a robust immunotherapy treatment strategy for the treatment of high-grade gliomas in humans, a number of key experimental limitations presented themselves during the course of this study. In Patient 1, FDA restrictions prevented the acquisition of a pre-CTL [^{18}F]FHBG scan, however, we have previously shown in a post-CTL [^{18}F]FHBG scan that CTL-associated radioactivity exquisitely corresponded to enhancing foci on MRI, not detectable by [^{18}F]FDG-PET (fig. S11) (16). Therefore, we believed that CTLs had likely properly migrated to the target tumor areas, but given that high-grade glioma cells in pre-CTL scans were [^{18}F]FHBG-positive in other patients, we were unable to confirm this hypothesis.

The CTL infusion techniques used in this study are also expected to play a role in the survival of CTLs in vivo and their homing to the tumor site. In Patient 3 (NCT01082926), the CTLs were injected using a slow infusion technique over several hours. This delivery technique resulted in cell clumping that may have reduced cell viability, however, [^{18}F]FHBG total activity was still increased 2.4-fold from 3.5 to 8.4 in this patient (fig. S9), reflecting the likely survival of a substantial proportion of these CTLs. The positioning of

the Rickham catheter tip next to the ventricular system may also affect optimal CTL trafficking to tumor sites. In Patients 4 and 5, the Rickham catheter tip was positioned next to the ventricular system. In these patients, CTLs likely diffused into the cerebrospinal fluid, as evidenced by the diffusion of [^{18}F]FHBG within the lateral ventricles in the post-CTL [^{18}F]FHBG scan, which was not observed on the pre-CTL scan (fig. S10A,B). These findings suggest that the dilution phenomenon might potentially affect the therapeutic effect by reducing the overall number of CTLs at the recurrent tumor site. On the other hand, this might be beneficial for patients whose tumors are located next to the ventricular system and are at higher risk of spinal leptomeningeal dissemination (30, 31). Nevertheless, these explanations require further validation.

The tumor vascular supply may also affect the ability to track CAR-engineered CTLs with [^{18}F]FHBG. In Patient 5, the recurrent glioma was adherent to the dura mater, which contributed to a rich vascular supply with disrupted blood-tumor barrier. As a consequence, intravenously injected [^{18}F]FHBG could readily diffuse from the leaky vascular supply into the tumor. In this patient, baseline [^{18}F]FHBG total activity was substantially higher at 23.1, compared to a mean total activity of 6.2 ± 2.9 for all other patients for whom a pre-CTL scan was available (n = 7 foci). It is highly plausible that elevated baseline [^{18}F]FHBG tumor uptake is a direct result of increased delivery and non-specific retention of the radiotracer in the tumor. Furthermore, high baseline [^{18}F]FHBG uptake on pre-CTL infusion scans may confound accurate measurement of CTL tracking. Indeed, [^{18}F]FHBG total activity in Patient 5 was increased by just 21% in the post-CTL infusion scan when compared to the baseline scan, at 28.1 and 23.1, respectively (fig. S12).

Discussion

Malignant gliomas are the most frequently occurring primary brain tumors and are associated with a very poor survival rate (32). Tremendous efforts have focused on the design of diagnostic and therapeutic tools for this devastating disease, among which targeted immunotherapy holds great promise (33). Unlike current conventional cancer treatments, the potential of immunotherapy resides in selectively targeting cancer cells while leaving healthy cells unharmed. One of the main immunotherapeutic methods under exploration is through CAR engineering of CTLs to become tumor-reactive and tumor-specific (34).

To fully validate immunotherapeutic strategies, it is crucial to monitor the viability, biodistribution, and trafficking of therapeutic cells to the site of the tumor. At present there is no means to assess the fate of these cells. Imaging via MRI, optical, or nuclear medicine-based techniques, however, has the potential to noninvasively monitor and track these cells in vivo. Two main approaches have been undertaken for cell tracking: direct and indirect labeling methods (35, 36). Direct labeling of cells involves incubation and retention of an imaging agent by the therapeutic cells which are injected into the subject, with the imaging agent monitored over a time course of hours to days. One example of a direct labeling method, using superparamagnetic iron oxide (SPIO)-labeled cells, has demonstrated great potential for the accurate assessment of image-guided cell injection into the tissue of interest (37).

Although they are relatively inexpensive and easy to perform, direct labeling methods are hampered by potential toxicity to the therapeutic cells (38). Moreover, the contrast agent becomes diluted upon cell division and is lost from the cells upon cell death, making image analysis difficult to interpret (39). To circumvent these issues, we and others have developed noninvasive indirect imaging reporter strategies to successfully track these cells (40–43). These methods enable imaging over the entire lifetime of the cell, with signal maintained after cell division, and provide information regarding cell viability (39). The majority of the signal is obtained from living cells because the production of the imaging reporter is dependent on translation of a gene into a functional protein, in a process requiring ATP. In this study, we demonstrated in humans that therapeutic CAR T cells can be detected noninvasively after intracranial adoptive transfer, through the PET imaging of a reporter gene.

Here, CTLs were engineered to express the tumor-targeting IL-13 zetakine CAR and the wild-type *HSV1-tk* reporter gene, with HSV1-TK expression monitored by [^{18}F]FHBG PET imaging. In cell culture, [^{18}F]FHBG uptake was 12-fold higher in *HSV1-tk*-expressing CTLs compared to naïve human T lymphocytes that were isolated from a human buffy coat. [^{18}F]FHBG incubation also had no effect on CTL proliferation rate in cell culture, presumably due to the low amount of mass tracer used. The functional and cytolytic activity of CTLs obtained from Patient 1 has been shown previously (18). For all other patients, insufficient tumor material was obtained at biopsy to enable primary GBM or patient-derived xenografts to be established in immunocompromised mice. We were therefore unable to assess functional activity of the CTLs against each patient's GBM cells.

[^{18}F]FHBG is a relatively poor substrate for mammalian thymidine kinases, resulting in low background accumulation in cells not expressing the *HSV1-tk* reporter gene, such as naïve human T lymphocytes and normal brain cells (22). Negligible brain-associated radioactivity was observed in [^{18}F]FHBG scans both before and after CTL infusions, with [^{18}F]FHBG not able to diffuse across an intact blood-brain barrier (BBB) (29), thereby providing an ideal low background signal. In glioma patients with a disrupted BBB, however, [^{18}F]FHBG accumulation in tumors was evident before CTL infusions. Retention of [^{18}F]FHBG in untreated tumors before CTL infusion may result from slow washout of the radiotracer from the resection cavity or be a consequence of off-target retention in the tumor cells. It was therefore vital to perform [^{18}F]FHBG imaging both before and after CTL infusions for accurate monitoring of this CAR T cell therapy strategy.

Because the location of the CTLs within the brain cavity were unknown, better imaging metrics were needed to replace single-voxel measurements such as SUV_{max} to define both the location and quantity of the therapeutic cells. We used a contouring algorithm based upon a set radioactivity threshold value relative to SUV_{max} to determine an accurate VOI. Through this method we could accurately assess not only tumor-associated CTLs, but also poorly targeted CTLs and CTLs that had targeted diffusely growing tumor cells undetected on contrast-enhanced MRI. For quantitation, we assessed [^{18}F]FHBG total activity within the generated ROI (SUV_{mean} × volume of interest) as an unbiased measure of [^{18}F]FHBG signal in a fixed volume region within the brain (namely the tumor) and in the setting where the [^{18}F]FHBG signal, and therefore CTLs, was widely dispersed after CTL infusions. This

metric is comparable to total lesion glycolysis used with [^{18}F]2-fluoro-2-deoxy-D-glucose ([^{18}F]FDG) PET, which is a more sensitive marker than SUV_{max} or SUV_{mean} for the evaluation of therapeutic response and prognosis (44–46).

The noninvasive imaging of genetically engineered CTLs for cancer immunotherapy held some specific challenges. Because [^{18}F]FHBG was the first PET reporter probe to receive an investigational new drug (IND) approval from the FDA (IND #61,880), strict regulations prevented repeat [^{18}F]FHBG scans before and after immunotherapy for the initial patient. This, coupled with the complexity of the immunotherapy strategy, markedly high cost (estimated at ~ $200,000 USD per patient), and limited access to this patient population restricted the number of patients who were enrolled in this study. In spite of these obstacles, a significant increase in [^{18}F]FHBG total activity representing CTL trafficking to tumor sites was observed across our patient cohort ($P = 0.014$; paired Wilcoxon test), highlighting the potential of this imaging strategy. It is unclear, however, whether IL-2-mediated changes in BBB permeability contributed to changes in [^{18}F]FHBG signal in the post-CTL scan. Moreover, we were unable to assess accurate delivery of CTLs to the tumor and its effect on differential [^{18}F]FHBG uptake. These variables will need to be evaluated in future studies. Although the absolute intrinsic uptake of [^{18}F]FHBG per cell remained relatively low, the mutant *HSV1-tk* reporter gene, *HSV1-sr39tk*, may provide increased sensitivity for detection through increased trapping of [^{18}F]FHBG in engineered cells in future clinical trials (23, 47). Finally, because of the limited number of patients enrolled on this study, it was not possible to link changes in [^{18}F]FHBG signal before and after CTL infusions to clinical outcome. Future work will need to link CTL trafficking and viability, as measured by [^{18}F]FHBG PET, to tumor response and patient survival. In summary, this work highlights an approach that uses a specific PET tracer to image *HSV1-tk* reporter gene expression in engineered CTLs to monitor CAR therapy for the treatment of high-grade gliomas.

Materials and methods

Study design

The primary research objective was to test the feasibility of [^{18}F]FHBG gene reporter imaging for the monitoring of therapeutic T cell distribution and viability in glioma patients. Patients from 18-70 years old with an average clinical status (a Karnofsky Performance Status > 60) and evidence of disease progression twelve weeks after the end of radiotherapy were included in this study. Exclusion criteria were a survival expectation of less than four weeks, any organ dysfunction, a large tumor requiring decompression surgery, a tumor located in the basal ganglia, thalamus, or brainstem, a patient treated for severe infection or recovering from major surgery, a history of IL-2 intolerance, and a history of ganciclovir and/or MRI contrast allergy or intolerance. Authors were not blinded to the results and no randomization was performed.

Patient recruitment

Seven patients (4 men, 3 women; mean age ± SD, 57 ± 8 years old) were prospectively enrolled from April 2006 to October 2013, in two separate clinical trials to evaluate the

safety and feasibility of intratumoral immunotherapy with CTLs (Table 1). Patients 1 and 2 were treated with autologous CTLs (NCT00730613) (17), whereas Patients 3-7 received allogeneic CTLs (NCT01082926). Patients included in this study were diagnosed with recurrent glioblastoma overexpressing the IL-13Rα2 receptor, thus allowing the recognition of malignant glioma cells by the genetically modified CTLs (17, 19, 48). It has previously been shown that patient prognosis and survival are inversely proportional to the abundance of tumor-associated IL-13Rα2 (25). Nevertheless, the presence of these specific targets helped to define patients who would likely benefit and respond to immunotherapy. No patient received additional radiotherapy or chemotherapy throughout this study. All patients were initially treated and followed up at the City of Hope, Duarte, California, USA. The Institutional Review Board and the local ethics committee approved all study protocols, and informed consent was obtained from each patient.

CTL engineering

The T-cell manufacturing process has been described previously in detail (17). For Patients 1-2: T-cells were expanded from clones that had been selected from genetically modified T-cells isolated from the patient's peripheral blood mononuclear cells (PBMC). A plasmid DNA construct encoding the *IL-13* zetakine CAR and the wild-type *HSV1-tk* genes under the transcriptional control of a modified human Elongation Factor-1α (EF-1α) promoter and the cytomegalovirus (CMV) immediate/early promoter, was transfected into the isolated cells using electroporation in a cell production facility at the City of Hope, Duarte, (California, USA). Hygromycin resistant CTLs were cloned in limiting dilution, then expanded using the rapid expansion method (REM) method to numbers in excess of 10^9 and subsequently cryopreserved (17). Following the diagnosis of tumor relapse the cryopreserved cells were thawed, REM expanded and formulated for intracranial infusion in 2 mL of preservative-free normal saline (PFNS). For Patients 3-7: The GRm13Z40-2 CTL line was derived from a healthy volunteer donor apheresis unit. The GRm13Z40-2 CTL line is an *ex vivo* expanded allogeneic genetically modified oligoclonal $CD8^+$ cytotoxic T lymphocyte line that expresses the IL-13 zetakine CAR and contains a biallelic deletion in the glucocorticoid receptor (GR) to confer steroid resistance. PBMC were subjected to electroporation to introduce plasmid IL-13 zetakine CAR DNA, followed by activation with monoclonal antibody Muromonab CD3 (30 ng/mL; trade name Orthoclone OKT3, marketed by Janssen-Cilag), *ex vivo* REM expansion (17), and selection in the presence of cytotoxic concentrations of hygromycin (0.2 mg/mL). Hygromycin-selected IL-13 zetakine CTLs were then subjected to transfection using the chimeric Ad5/35 adenovirus encoding a zinc finger nuclease (ZFN) pair that targets the human GR, which led to permanent disruption of the reading frame. Adenovirus transfected IL-13 zetakine CTLs were subjected to selection in dexamethasone. Surviving T cells underwent large-scale REM expansion followed by cryopreservation to generate an allogeneic IL-13 zetakine CTL bank. Following the diagnosis of recurrent GBM the cryopreserved cells were thawed and formulated for intracranial infusion in 2 mL of preservative-free normal saline (PFNS).

Infusion methods

Patients 1-2 underwent craniotomy for tumor resection and placement of Rickham reservoir and catheter for CTL injection, as previously detailed (17). These patients were treated with

a series of twelve infusions of autologous CTLs (each over 10 minutes) on days 1, 3, and 5 over a period of 5 weeks, with a break on week 3. If the initial dose of 1×10^7 CTLs was tolerated, subsequent infusions were increased to 5×10^7 and then 1×10^8 autologous CTLs per injection. Patients 3-7 had unresectable recurrent glioblastoma. These patients underwent stereotactic tumor biopsy and insertion of Rickham reservoir/catheter for intratumoral CTL infusion. These patients were treated with a series of four infusions of 1×10^8 allogeneic CTLs along with escalating doses of recombinant human IL-2 to prolong the survival of CTLs (49). Allogeneic CTLs were infused on days 1 and 3 for two consecutive weeks; IL-2 was infused on days 2, 3, 4, and 5 of the first week (2500 IU/day) and on days 1, 2, 3, 4, and 5 of the second week (5000 IU/day) (table S3). In Patient 3, CTLs and IL-2 were administered directly into the tumor cavity by convection-enhanced delivery, which is a drug delivery strategy designed to circumvent the central nervous system defense system and improve drug distribution (50). It allows for delivery of high concentrations of therapeutic agents directly into brain tumors and surrounding parenchyma with minimal systemic toxicity. Because of cell clumping associated with slow infusion, CTL delivery technique was switched to a “manual push” technique over 10 minutes in Patients 4-7.

Clinical assessment

Before each [^{18}F]FHBG scan, we obtained a physical exam, a 12-lead electrocardiogram (ECG), vital signs (blood pressure, heart rate, respiratory rate, body temperature, and blood oxygenation), blood sampling (for complete blood chemistries, complete metabolic panel, international normalized ratio, and activated partial thromboplastin time), and urine (for urine analysis and pregnancy test, if needed). These values were used as a baseline. The patients’ routine medications and medical history were also recorded. Vital signs were taken at 5, 10, 15, 60, and 120 minutes after [^{18}F]FHBG injection. ECGs were monitored every 15 minutes up to 120 minutes after the tracer injection and were analyzed for PQ/QRS and QT changes.

After the PET scan was completed, another set of vital signs and ECG were collected. Within 24 hours of the scan, the participants returned to the clinic, and vital signs and ECG were again collected, as well as blood and urine samples. Seven days later, a similar assessment was performed in addition to a neuropsychological test (mini mental state examination) that was also performed at baseline. Any adverse events noted by the members of the research team or the participants during the whole procedure were recorded for up to a week during follow-up.

Imaging studies

9-[4-[^{18}F]fluoro-3-(hydroxymethyl)butyl]guanine, or [^{18}F]FHBG, was synthesized as previously described (22). The mean [^{18}F]FHBG activity injected was 259 ± 7 MBq (7.0 ± 0.2 mCi), with no significant differences between pre- and post-CTL infusion PET scans ($P > 0.05$). The maximum amount of unlabeled product was less than 2 μg, and the specific activity was greater than 37Gbq/μmol (22).

The tracer was administered as a bolus injection over less than 5 seconds via a hand or an arm vein. Approximately two hours after intravenous injection of [^{18}F]FHBG, PET images

were obtained from the skull vertex to mid-thighs. Scans for patients 1-2 were performed with a standalone PET scanner (Siemens ECAT EXACT™ HR+ PET scanner; CTI PET Systems, Inc.). [^{18}F]FHBG PET scans, at 7 minutes per bed position, were performed for both Patients 1-2, but no baseline scan was done for Patient 1.(16). In addition, delayed brain PET images were obtained for Patient 1. After the emission scan, the patient underwent a transmission scan for 3 minutes per bed position, using 3 rotating ^{68}Ge rod sources. PET images were reconstructed with OSEM algorithm with attenuation correction on a 128 × 128 matrix size. The images for patients 3-5 images were obtained with a PET/CT scanner (Siemens Biograph TruePoint 64-slice). A topogram scan (120 kVp, 35 mAs) was acquired, followed by a low-dose non-contrast CT (helical mode, rotation 0.5 sec, slice thickness 5.0 mm, 120 kVp, 100 mA) for attenuation correction and anatomic localization. PET images were obtained in 3D mode for 7 minutes per bed position, using an iterative reconstruction algorithm (2 iterations and 24 subsets) on a 168 × 168 matrix size and a Gaussian filter cut-off of 5.0 mm. Images for Patients 6 and 7 were obtained on another PET/CT scanner (Siemens Biograph mCT 64-slice). All image protocols were similar to those on the Biograph TruePoint, except for the matrix size, which was larger at 200 × 200. All PET images were decay corrected to the time of injection. Each patient was asked to void their bladder before each scan to reduce their total radiation exposure. All [^{18}F]FHBG PET images were obtained at the University of California, Los Angeles, California, USA. All PET scanners were fully calibrated and tested for quantitative accuracy; these procedures were performed according to the manufacturer's recommendations.

In addition, brain [^{18}F]FDG and MRI were performed before and after CTL infusions, using standard oncological protocols. These images were obtained at City of Hope, Duarte California, USA, and were scheduled within a few days of the [^{18}F]FHBG imaging.

Image analysis

All data analyses were performed at Stanford University (California, USA), University College London (London, UK), and Hôpital de la Cité-de-la-Santé de Laval (Québec, Canada). [^{18}F]FHBG images were co-registered to MRI images on MIM Encore v6.4, MIM Software and on Siemens Inveon v4.2, Research Workplace. Automatic image registration was applied initially, and manual positioning was performed as necessary. [^{18}F]FHBG images were analyzed in all axial planes and with different thresholds to detect subtle abnormal uptake. Standardized uptake values (SUVs) were measured in different areas using a three-dimensional 50 mm diameter spherical volume of interest for healthy tissue. Values were obtained for the left ventricle of the heart (referred to as blood pool); the left and right lung parenchyma; the right hepatic dome (referred to as liver); the left and right quadriceps musculature (referred to as thigh); the bone marrow; the left and right frontal lobes, parietal lobes, temporal lobes, occipital lobes, and the cerebellum (table S2). Activity within all brain areas except the site of surgical resection or tumor recurrence, was averaged to represent the background brain uptake. An irregular three-dimensional volume of interest was drawn over the abnormal uptake area in the brain (tumor recurrence and/or CTL foci): we used the native volume growth algorithm from MIM Encore 6.4, MIM Software, and we applied different thresholds for delineation. A 10% threshold of SUV_{max} was initially drawn, and 10% increments were subsequently applied until 90% of SUV_{max} was obtained.

MRI and [^{18}F]FHBG PET images were always compared side-by-side to help in visual adjustment of boundaries. In addition, MRI and [^{18}F]FHBG PET images were fused together to optimally visualize the uptake area. To do this, rigid-body registration with rotations was initially applied, followed by deformable registration. In most cases, the delineation on [^{18}F]FHBG PET images followed the enhancing boundaries visualized on T_1 post-gadolinium sequence on MRI images. For treatment response, we always considered the background activity as part of baseline normal brain uptake. Therefore, we subtracted background activity from the activity measured in each volume of interest.

Different strategies were used for evaluating therapy response: we used SUV_{max}, SUV_{mean}, three-dimensional volumes encompassing the tumor, individual voxel histogram analysis, and a parameter which takes into consideration the [^{18}F]FHBG concentration and the volume of interest. This parameter, referred to as total activity, corresponds to the SUV_{mean} multiplied by the volume of interest. To calculate the percentage of signal change between two scans, we used a formula that accounted for background activity in the brain:

$$\frac{(post\ CTL\ SUV\ lesion\ -\ SUV\ background)\ -\ (pre\ CTL\ SUV\ lesion\ -\ SUV\ background)}{pre\ CTL\ SUV\ lesion\ -\ SUV\ background}\times 100$$

Movie rendering was performed with Amira v5.2.2, Visage Imaging Inc.

Assessment of FHBG toxicity to transduced CTLs

Patient-derived CTLs: GRm13Z40 (HD040-IL13z-ZFN) – Control cell ID# cJ05105 and WCB-031-4C11-01 (UPN-031-IL13-zeta_DIIHyTK-pMG (pj00429#7)Cl.4C11) Cell ID# cj02331 were obtained from the T cell therapeutics lab at City of Hope Hospital, Duarte, CA as frozen vials. The CTLs were recovered in RPMI medium with *L*-glutamine and Hepes. Human IL-2 (50 units/mL) was added as a supplement. 15,000 cells for each cell type were plated in a 96 well tissue culture dish in RPMI medium. For the cells that needed to be exposed to the tracer, 7.4 kBq of FHBG was added to each well. 1 h after exposure to tracer, cells were washed with PBS twice and either lysed for counting accumulated radioactivity or plated in medium for an additional 24 h and 48 h. Viability assessment was performed using the Presto Blue assay as per the manufacturer's instructions (Thermofisher). Presto Blue uses the reducing environment of living cells to quantify viability. In brief, the desired volume of Presto Blue was added to the cells to a final concentration of 10%. The accumulated fluorescence was quantified using a microplate reader (excitation 540 nm, emission 600 nm), 30 min and 1 h after the addition of Presto Blue.

Statistical analysis

Statistical analysis was performed in Microsoft Excel 2010 v14.0.6 and GraphPad Prism Software v.5.0. Values were expressed as mean ± standard deviation (SD). To compare uptake in healthy organs before and after CTL infusions, and when comparing the effect of [^{18}F]FHBG incubation on CTL proliferation rate, the Student paired *t*-test was used. For comparison of [^{18}F]FHBG total activity measurement in lesions before and after CTL infusions for all patients, a paired Wilcoxon test was used. Probability values less than 0.05 were considered as statistically significant.

Supplementary Material

Refer to Web version on PubMed Central for supplementary material.

Acknowledgements

The authors would like to thank Gayatri Gowrishankar, Xinrui Yan, Aileen Hoehne and Robert Reeves for technical assistance.

Funding: This work was supported in part by NCI ICMIC P50CA114747 (SSG), NCI RO1 CA082214 (SSG), NCI RO1 CA135486 (SSG), the Ben & Catherine Ivy Foundation (SSG), NCI R01 CA155769 (BB), NCI R21 NS081594 (BB), NCI R21 CA189223 (BB), and Sangamo Biosciences. THW was supported in part by a Sir Henry Dale Fellowship jointly funded by the Wellcome Trust and the Royal Society (Grant Number 107610/Z/15/Z).

References

1. Vanneman M, Dranoff G. Combining immunotherapy and targeted therapies in cancer treatment. Nat Rev Cancer. 2012; 12:237–251. [PubMed: 22437869]
2. Qi CJ, Ning YL, Han YS, Min HY, Ye H, Zhu YL, Qian KQ. Autologous dendritic cell vaccine for estrogen receptor (ER)/progestin receptor (PR) double-negative breast cancer. Cancer Immunol Immunother. 2012; 61:1415–1424. [PubMed: 22290073]
3. Grupp SA, Kalos M, Barrett D, Aplenc R, Porter DL, Rheingold SR, Teachey DT, Chew A, Hauck B, Wright JF, Milone MC, et al. Chimeric antigen receptor-modified T cells for acute lymphoid leukemia. N Engl J Med. 2013; 368:1509–1518. [PubMed: 23527958]
4. Hodi FS, O'Day SJ, McDermott DF, Weber RW, Sosman JA, Haanen JB, Gonzalez R, Robert C, Schadendorf D, Hassel JC, Akerley W, et al. Improved survival with ipilimumab in patients with metastatic melanoma. N Engl J Med. 2010; 363:711–723. [PubMed: 20525992]
5. Kelderman S, Schumacher TN, Haanen JB. Acquired and intrinsic resistance in cancer immunotherapy. Mol Oncol. 2014; 8:1132–1139. [PubMed: 25106088]
6. Pardoll DM. The blockade of immune checkpoints in cancer immunotherapy. Nat Rev Cancer. 2012; 12:252–264. [PubMed: 22437870]
7. Beltinger C, Kurz E, Bohler T, Schrappe M, Ludwig WD, Debatin KM. CD95 (APO-1/Fas) mutations in childhood T-lineage acute lymphoblastic leukemia. Blood. 1998; 91:3943–3951. [PubMed: 9573033]
8. Curiel TJ, Coukos G, Zou L, Alvarez X, Cheng P, Mottram P, Evdemon-Hogan M, Conejo-Garcia JR, Zhang L, Burow M, Zhu Y, et al. Specific recruitment of regulatory T cells in ovarian carcinoma fosters immune privilege and predicts reduced survival. Nat Med. 2004; 10:942–949. [PubMed: 15322536]
9. Dudley ME, Gross CA, Langhan MM, Garcia MR, Sherry RM, Yang JC, Phan GQ, Kammula US, Hughes MS, Citrin DE, Restifo NP, et al. CD8+ enriched “young” tumor infiltrating lymphocytes can mediate regression of metastatic melanoma. Clin Cancer Res. 2010; 16:6122–6131. [PubMed: 20668005]
10. Finke LH, Wentworth K, Blumenstein B, Rudolph NS, Levitsky H, Hoos A. Lessons from randomized phase III studies with active cancer immunotherapies--outcomes from the 2006 meeting of the Cancer Vaccine Consortium (CVC). Vaccine. 2007; 2(25 Suppl):B97–B109.
11. Prieto PA, Yang JC, Sherry RM, Hughes MS, Kammula US, White DE, Levy CL, Rosenberg SA, Phan GQ. CTLA-4 blockade with ipilimumab: long-term follow-up of 177 patients with metastatic melanoma. Clin Cancer Res. 2012; 18:2039–2047. [PubMed: 22271879]
12. Eisenhauer EA, Therasse P, Bogaerts J, Schwartz LH, Sargent D, Ford R, Dancey J, Arbuck S, Gwyther S, Mooney M, Rubinstein L, et al. New response evaluation criteria in solid tumours: revised RECIST guideline (version 1.1). Eur J Cancer. 2009; 45:228–247. [PubMed: 19097774]
13. Brindle K. New approaches for imaging tumour responses to treatment. Nat Rev Cancer. 2008; 8:94–107. [PubMed: 18202697]
14. Wolchok JD, Hoos A, O'Day S, Weber JS, Hamid O, Lebbe C, Maio M, Binder M, Bohnsack O, Nichol G, Humphrey R, et al. Guidelines for the evaluation of immune therapy activity in solid

Europe PMC Funders Author Manuscripts

tumors: immune-related response criteria. Clin Cancer Res. 2009; 15:7412–7420. [PubMed: 19934295]

15. Nishino M, Giobbie-Hurder A, Gargano M, Suda M, Ramaiya NH, Hodi FS. Developing a common language for tumor response to immunotherapy: immune-related response criteria using unidimensional measurements. Clin Cancer Res. 2013; 19:3936–3943. [PubMed: 23743568]
16. Yaghoubi SS, Jensen MC, Satyamurthy N, Budhiraja S, Paik D, Czernin J, Gambhir SS. Noninvasive detection of therapeutic cytolytic T cells with 18F-FHBG PET in a patient with glioma. Nat Clin Pract Oncol. 2009; 6:53–58. [PubMed: 19015650]
17. Brown CE, Badie B, Barish ME, Weng L, Ostberg JR, Chang WC, Naranjo A, Starr R, Wagner J, Wright C, Zhai Y, et al. Bioactivity and Safety of IL13Ralpha2-Redirected Chimeric Antigen Receptor CD8+ T Cells in Patients with Recurrent Glioblastoma. Clin Cancer Res. 2015; 21:4062–4072. [PubMed: 26059190]
18. Brown CE, Starr R, Aguilar B, Shami AF, Martinez C, D'Apuzzo M, Barish ME, Forman SJ, Jensen MC. Stem-like tumor-initiating cells isolated from IL13Ralpha2 expressing gliomas are targeted and killed by IL13-zetakine-redirected T Cells. Clin Cancer Res. 2012; 18:2199–2209. [PubMed: 22407828]
19. Kahlon KS, Brown C, Cooper LJ, Raubitschek A, Forman SJ, Jensen MC. Specific recognition and killing of glioblastoma multiforme by interleukin 13-zetakine redirected cytolytic T cells. Cancer Res. 2004; 64:9160–9166. [PubMed: 15604287]
20. Yazawa K, Fisher WE, Brunicardi FC. Current progress in suicide gene therapy for cancer. World J Surg. 2002; 26:783–789. [PubMed: 11948367]
21. Yaghoubi SS, Barrio JR, Namavari M, Satyamurthy N, Phelps ME, Herschman HR, Gambhir SS. Imaging progress of herpes simplex virus type 1 thymidine kinase suicide gene therapy in living subjects with positron emission tomography. Cancer Gene Ther. 2005; 12:329–339. [PubMed: 15592447]
22. Yaghoubi SS, Gambhir SS. PET imaging of herpes simplex virus type 1 thymidine kinase (HSV1-tk) or mutant HSV1-sr39tk reporter gene expression in mice and humans using [18F]FHBG. Nat Protoc. 2006; 1:3069–3075. [PubMed: 17406570]
23. Gambhir SS, Bauer E, Black ME, Liang Q, Kokoris MS, Barrio JR, Iyer M, Namavari M, Phelps ME, Herschman HR. A mutant herpes simplex virus type 1 thymidine kinase reporter gene shows improved sensitivity for imaging reporter gene expression with positron emission tomography. Proc Natl Acad Sci U S A. 2000; 97:2785–2790. [PubMed: 10716999]
24. Gambhir SS, Herschman HR, Cherry SR, Barrio JR, Satyamurthy N, Toyokuni T, Phelps ME, Larson SM, Balatoni J, Finn R, Sadelain M, et al. Imaging transgene expression with radionuclide imaging technologies. Neoplasia. 2000; 2:118–138. [PubMed: 10933072]
25. Brown CE, Warden CD, Starr R, Deng X, Badie B, Yuan YC, Forman SJ, Barish ME. Glioma IL13Ralpha2 is associated with mesenchymal signature gene expression and poor patient prognosis. PLoS One. 2013; 8:e77769. [PubMed: 24204956]
26. Debinski W, Gibo DM, Hulet SW, Connor JR, Gillespie GY. Receptor for interleukin 13 is a marker and therapeutic target for human high-grade gliomas. Clin Cancer Res. 1999; 5:985–990. [PubMed: 10353730]
27. Dubey P, Su H, Adonai N, Du S, Rosato A, Braun J, Gambhir SS, Witte ON. Quantitative imaging of the T cell antitumor response by positron-emission tomography. Proc Natl Acad Sci U S A. 2003; 100:1232–1237. [PubMed: 12547911]
28. Kim YJ, Dubey P, Ray P, Gambhir SS, Witte ON. Multimodality imaging of lymphocytic migration using lentiviral-based transduction of a tri-fusion reporter gene. Mol Imaging Biol. 2004; 6:331–340. [PubMed: 15380743]
29. Yaghoubi S, Barrio JR, Dahlbom M, Iyer M, Namavari M, Satyamurthy N, Goldman R, Herschman HR, Phelps ME, Gambhir SS. Human pharmacokinetic and dosimetry studies of [(18)F]FHBG: a reporter probe for imaging herpes simplex virus type-1 thymidine kinase reporter gene expression. J Nucl Med. 2001; 42:1225–1234. [PubMed: 11483684]
30. Shakur SF, Bit-Ivan E, Watkin WG, Merrell RT, Farhat HI. Multifocal and multicentric glioblastoma with leptomeningeal gliomatosis: a case report and review of the literature. Case Rep Med. 2013; 2013:132679. [PubMed: 24381594]

31. Bae JS, Yang SH, Yoon WS, Kang SG, Hong YK, Jeun SS. The clinical features of spinal leptomeningeal dissemination from malignant gliomas. J Korean Neurosurg Soc. 2011; 49:334–338. [PubMed: 21887390]
32. Ahmed R, Oborski MJ, Hwang M, Lieberman FS, Mountz JM. Malignant gliomas: current perspectives in diagnosis, treatment, and early response assessment using advanced quantitative imaging methods. Cancer Manag Res. 2014; 6:149–170. [PubMed: 24711712]
33. Bielamowicz K, Khawja S, Ahmed N. Adoptive cell therapies for glioblastoma. Front Oncol. 2013; 3:275. [PubMed: 24273748]
34. Schuessler A, Smith C, Beagley L, Boyle GM, Rehan S, Matthews K, Jones L, Crough T, Dasari V, Klein K, Smalley A, et al. Autologous T-cell therapy for cytomegalovirus as a consolidative treatment for recurrent glioblastoma. Cancer Res. 2014; 74:3466–3476. [PubMed: 24795429]
35. Harisinghani MG, Barentsz J, Hahn PF, Deserno WM, Tabatabaei S, van de Kaa CH, de la Rosette J, Weissleder R. Noninvasive detection of clinically occult lymph-node metastases in prostate cancer. N Engl J Med. 2003; 348:2491–2499. [PubMed: 12815134]
36. Kircher MF, Gambhir SS, Grimm J. Noninvasive cell-tracking methods. Nat Rev Clin Oncol. 2011; 8:677–688. [PubMed: 21946842]
37. Bulte JW. In vivo MRI cell tracking: clinical studies. AJR Am J Roentgenol. 2009; 193:314–325. [PubMed: 19620426]
38. Botti C, Negri DR, Seregni E, Ramakrishna V, Arienti F, Maffioli L, Lombardo C, Bogni A, Pascali C, Crippa F, Massaron S, Remonti F, Nerini-Molteni S, Canevari S, Bombardieri E. Comparison of three different methods for radiolabelling human activated T lymphocytes. Eur J Nucl Med. 1997; 24:497–504. [PubMed: 9142729]
39. Kurtz DM, Gambhir SS. Tracking cellular and immune therapies in cancer. Adv Cancer Res. 2014; 124:257–296. [PubMed: 25287692]
40. Luker GD, Luker KE, Sharma V, Pica CM, Dahlheimer JL, Ocheskey JA, Fahrner TJ, Milbrandt J, Piwnica-Worms D. In vitro and in vivo characterization of a dual-function green fluorescent protein--HSV1-thymidine kinase reporter gene driven by the human elongation factor 1 alpha promoter. Mol Imaging. 2002; 1:65–73. [PubMed: 12920846]
41. Min JJ, Gambhir SS. Molecular imaging of PET reporter gene expression. Handb Exp Pharmacol. 2008:277–303. [PubMed: 18626607]
42. Soghomonyan S, Hajitou A, Rangel R, Trepel M, Pasqualini R, Arap W, Gelovani JG, Alauddin MM. Molecular PET imaging of HSV1-tk reporter gene expression using [18F]FEAU. Nat Protoc. 2007; 2:416–423. [PubMed: 17406603]
43. Tjuvajev JG, Doubrovin M, Akhurst T, Cai S, Balatoni J, Alauddin MM, Finn R, Bornmann W, Thaler H, Conti PS, Blasberg RG. Comparison of radiolabeled nucleoside probes (FIAU, FHBG, and FHPG) for PET imaging of HSV1-tk gene expression. J Nucl Med. 2002; 43:1072–1083. [PubMed: 12163634]
44. Olivier A, Petyt G, Cortot A, Scherpereel A, Hossein-Foucher C. Higher predictive value of tumour and node [18F]-FDG PET metabolic volume and TLG in advanced lung cancer under chemotherapy. Nucl Med Commun. 2014
45. Pak K, Cheon GJ, Nam HY, Kim SJ, Kang KW, Chung JK, Kim EE, Lee DS. Prognostic Value of Metabolic Tumor Volume and Total Lesion Glycolysis in Head and Neck Cancer: A Systematic Review and Meta-Analysis. J Nucl Med. 2014; 55:884–890. [PubMed: 24752671]
46. Moon SH, Hyun SH, Choi JY. Prognostic significance of volume-based PET parameters in cancer patients. Korean J Radiol. 2013; 14:1–12. [PubMed: 23323025]
47. Yaghoubi SS, Couto MA, Chen CC, Polavaram L, Cui G, Sen L, Gambhir SS. Preclinical safety evaluation of 18F-FHBG: a PET reporter probe for imaging herpes simplex virus type 1 thymidine kinase (HSV1-tk) or mutant HSV1-sr39tk's expression. J Nucl Med. 2006; 47:706–715. [PubMed: 16595506]
48. Sengupta S, Thaci B, Crawford AC, Sampath P. Interleukin-13 Receptor Alpha 2-Targeted Glioblastoma Immunotherapy. Biomed Res Int. 2014; 2014:952128. [PubMed: 25247196]
49. Grimm EA, Jacobs SK, Lanza LA, Melin G, Roth JA, Wilson DJ. Interleukin 2-activated cytotoxic lymphocytes in cancer therapy. Symp Fundam Cancer Res. 1986; 38:209–219. [PubMed: 3489259]

50. Juratli TA, Schackert G, Krex D. Current status of local therapy in malignant gliomas--a clinical review of three selected approaches. Pharmacol Ther. 2013; 139:341–358. [PubMed: 23694764]

Europe PMC Funders Author Manuscripts

Europe PMC Funders Author Manuscripts

One Sentence summary

Positron emission tomography gene reporter imaging can be used to monitor the trafficking and homing of therapeutic cytotoxic T lymphocytes to tumor sites in glioma patients.

Europe PMC Funders Author Manuscripts

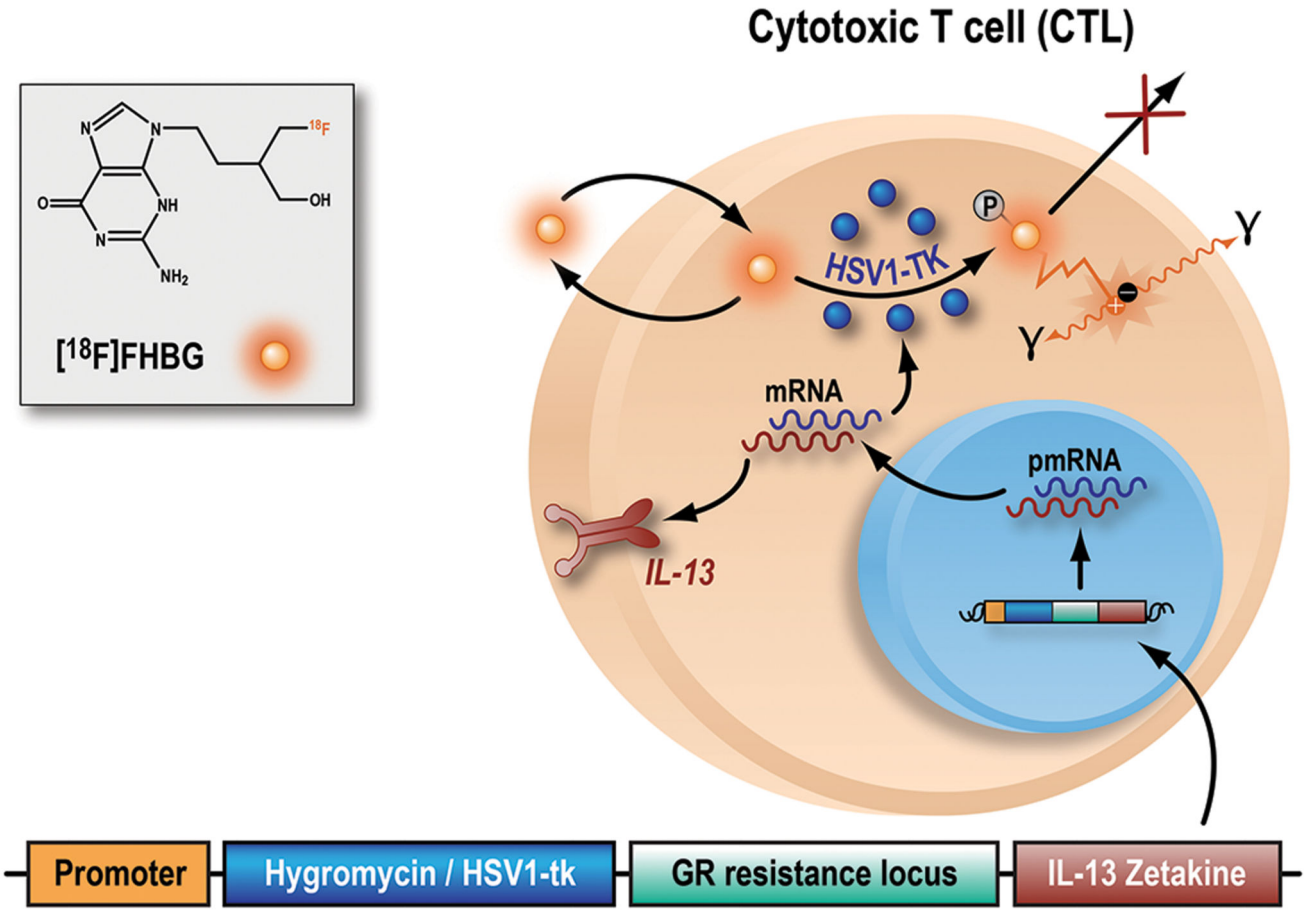

Fig. 1. The herpes simplex virus type-1 thymidine kinase gene (*HSV1-tk*) complex and monitoring by [^{18}F]FHBG.

The herpes simplex virus type-1 thymidine kinase gene (*HSV1-tk*) complex is a genetically modified structure that was transfected into either autologous or allogeneic CTLs. This complex expresses a fusion protein consisting of a selective gene (hygromycin resistance locus) for adequate in vitro expansion of the CTL line; a PET reporter gene and safety gene, *HSV1-tk*; a glucocorticoid receptor (GR) resistance locus for improving CTL survival despite the high doses of steroids routinely given to high-grade glioma patients; and a IL-13 zetakine domain which is a chimeric receptor that enables glioma cell recognition by CTLs. CTL transfection was performed by electroporation. Inside the transfected cells, *HSV1-tk* is transcribed and translated to produce the HSV1-TK enzyme. [^{18}F]FHBG is a labeled analog of penciclovir and substrate for HSV1-TK. In the presence of HSV1-TK, the radiolabeled probe is phosphorylated and trapped within the cell. The magnitude of [^{18}F]FHBG signal reflects the activity of HSV1-TK enzyme and thus *HSV1-tk* gene expression. Abbreviation: pmRNA, pre-messenger RNA.

Europe PMC Funders Author Manuscripts

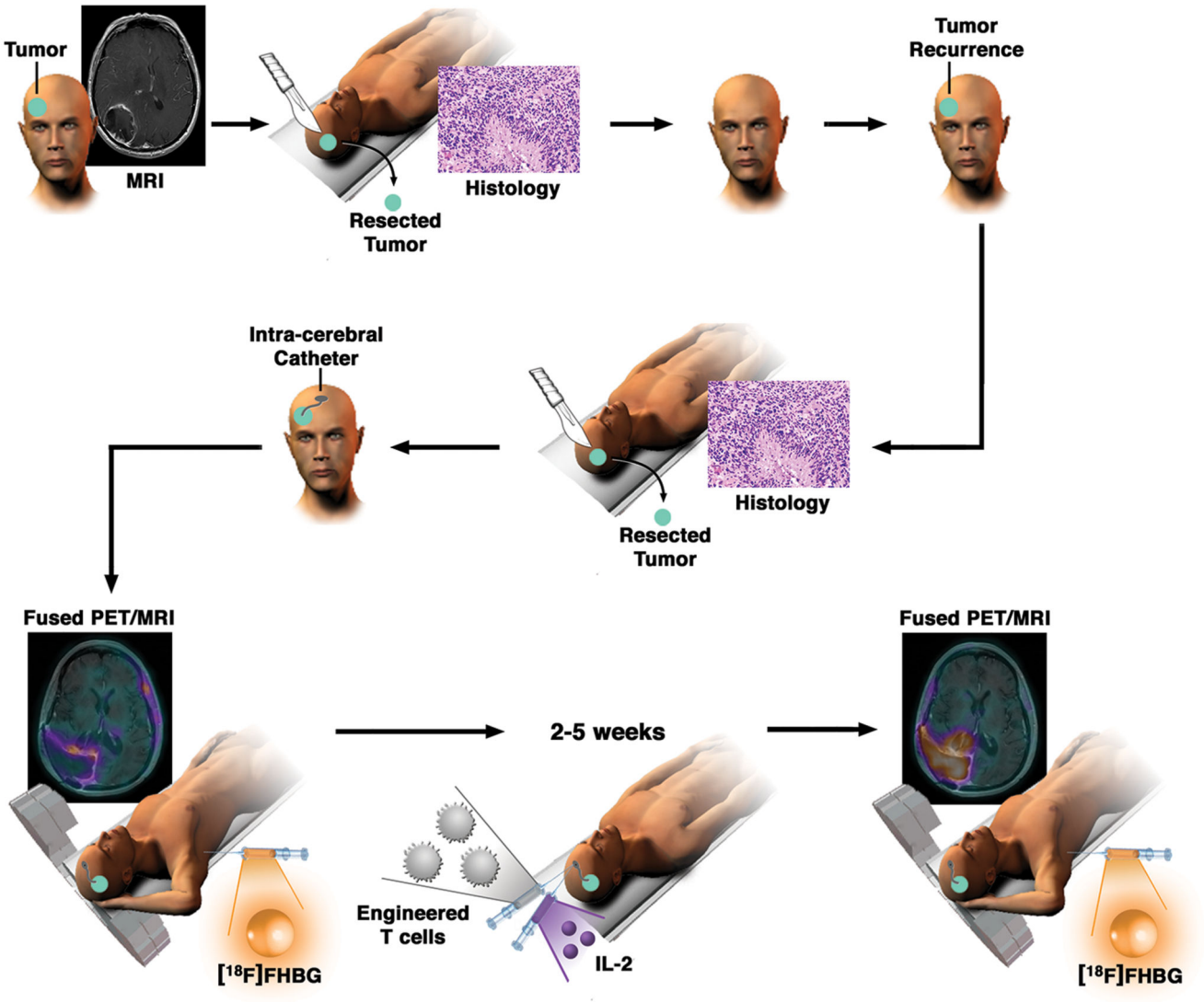

Fig. 2. Schematic demonstrating the workup and monitoring of CTL infusion after an initial treatment for high-grade glioma.

After enrollment in this study and upon tumor recurrence, an intracerebral Rickham catheter was installed for repetitive infusions of CTLs. Each patient underwent [^{18}F]FHBG PET and MRI before and after CTL infusions. In addition, IL-2 was administered at regular intervals to further increase the survival and enhance the potency of the administered CTLs. CTL distribution was imaged by measuring changes in tumoral [^{18}F]FHBG accumulation before and after infusions of cells.

Europe PMC Funders Author Manuscripts

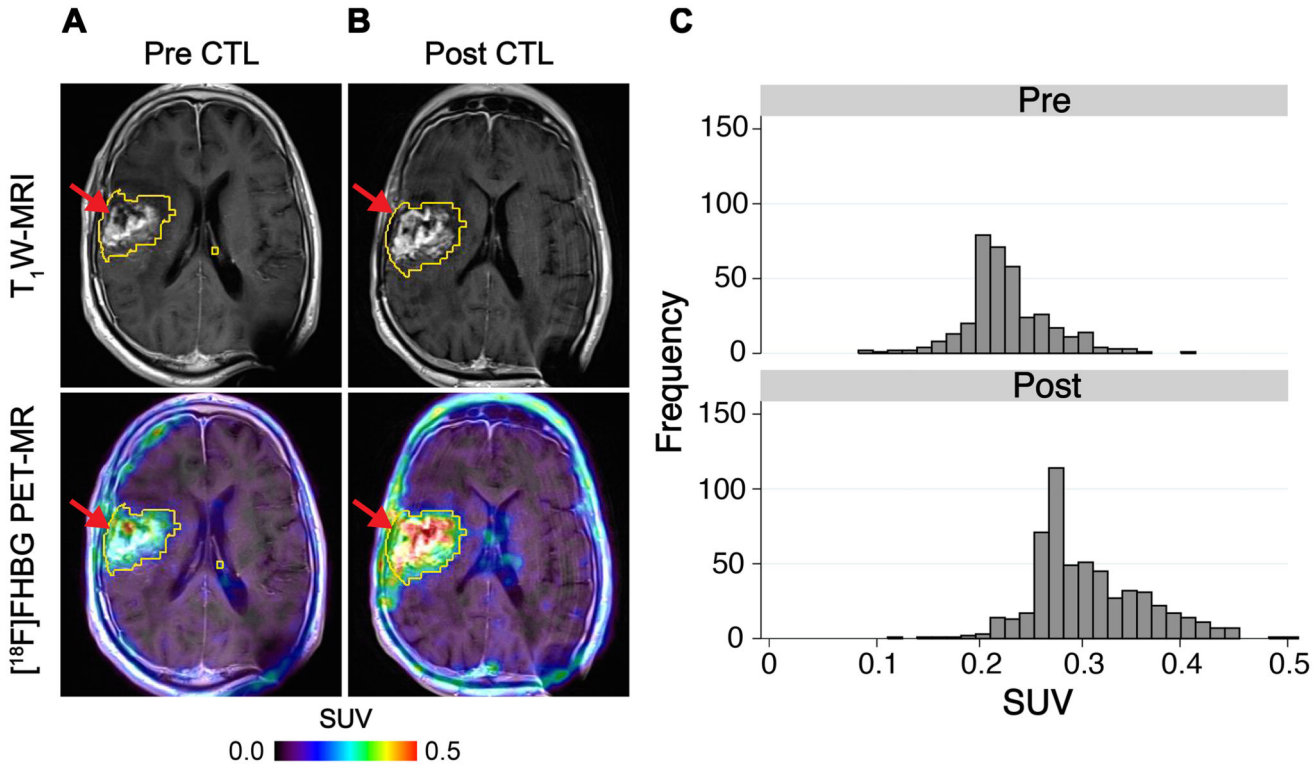

Fig. 3. Tumor-associated CTL imaging with [^{18}F]FHBG.

[^{18}F]FHBG PET imaging was performed in a 66 year-old male (Patient 6) with a recurrent right frontoparietal glioblastoma before (**A**) and one week after (**B**) CTL infusions. Allogeneic CTLs and IL-2 were injected intratumorally (red arrows) as described in Materials and Methods. Tumor recurrence was monitored by T_1-weighted (T_1W) MRI (top panels). [^{18}F]FHBG PET images were fused with MRI images (bottom panels), and 3D volumes of interest were drawn using a 50% [^{18}F]FHBG SUV_{max} threshold, outlined in yellow. (**C**) Voxel-wise analysis of [^{18}F]FHBG SUV in pre- and post-CTL infusion scans.

Europe PMC Funders Author Manuscripts

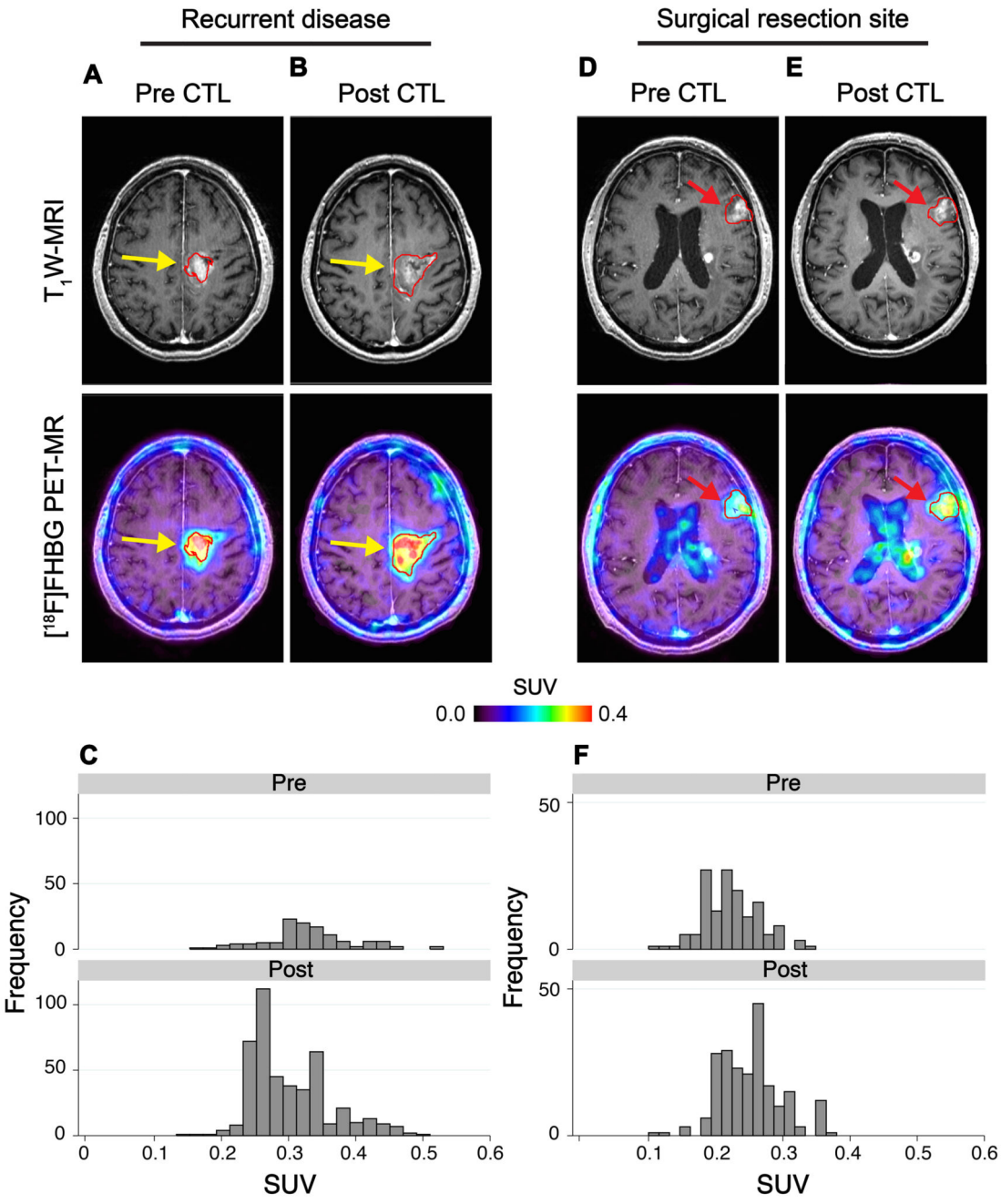

Fig. 4. [^{18}F]FHBG PET imaging in recurrent disease and at untreated tumor sites.

[^{18}F]FHBG PET imaging was performed in a 60 year-old male (Patient 7) with multifocal left hemispheric glioma. CTLs were injected into the medial left frontal lobe tumor (yellow arrows). (**A**) Tumor size was monitored by T_1-weighted (T_1W) contrast-enhanced MRI (top left panels). [^{18}F]FHBG PET images were fused with MRI images (bottom left panels), and 3D volumes of interest were drawn using a 50% [^{18}F]FHBG SUV_{max} threshold, outlined in red. (**B**) MRI and [^{18}F]FHBG PET-MR images one week after CTL infusions. (**C**) Voxel-wise analysis of [^{18}F]FHBG total radioactivity in pre- and post-CTL infusion scans.

[^{18}F]FHBG activity was additionally assessed in a non-injected tumor focus (red arrows) before (**D**) and after (**E**) CTL infusions, with voxel-wise analysis of this lesion performed for comparison (**F**).

Europe PMC Funders Author Manuscripts

Europe PMC Funders Author Manuscripts

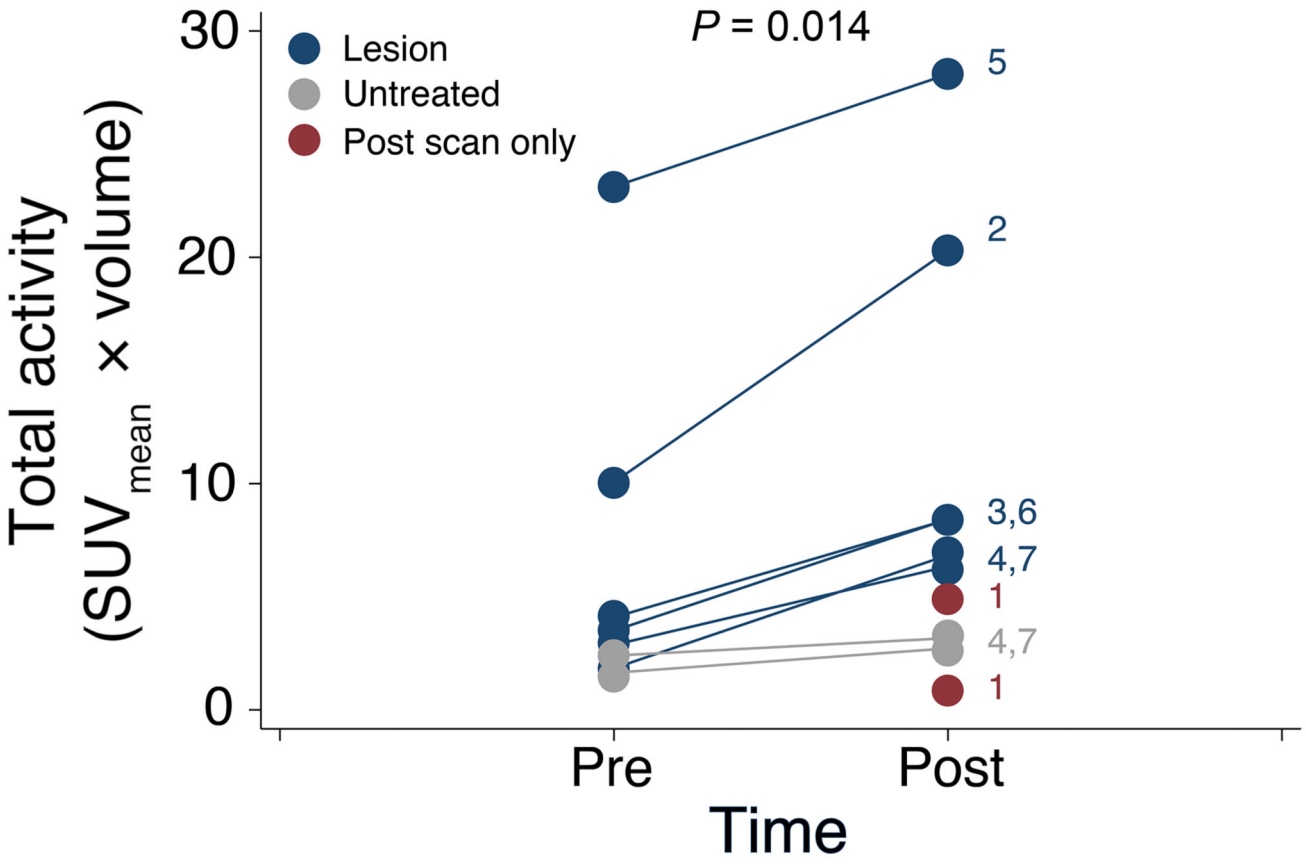

Fig. 5. Changes in [^{18}F]FHBG total activity in patients after CTL infusions.

The total activity (SUV_{mean} × uptake volume) was measured for each patient on pre- and post-CTL [^{18}F]FHBG scans, with the VOI obtained after a 50% SUV_{max} threshold. Clinically-confirmed sites of tumor recurrence that received CTL infusions are indicated in blue. Non-injected tumor foci in patients with multifocal disease are indicated in gray. In Patient 1, for whom no pre-CTL scan was available, the total activity values for the two tumor foci are shown in red. For reference, patient numbers are indicated next to the post-CTL [^{18}F]FHBG values. The increase in [^{18}F]FHBG signal after CTL infusion was statistically significant ($P = 0.014$; paired Wilcoxon test).

Table 1

Imaging and demographic data for all seven patients enrolled in this study.

Patient #	1	2	3	4	5	6	7
Gender	M	F	F	M	F	M	M
Age (years)	57	41	61	62	53	66	60
CTL type	autologous	autologous	allogeneic	allogeneic	allogeneic	allogeneic	allogeneic
Histology	Glioma	Glioma	Glioma	Glioma	Glioma	Glioma	Glioma
IL13Rα2 expression	N/A	N/A	2-3+ / 80%	2-3+ / 80%	2-3+ / 70%	2+ / 60%	2+ / 90%
Site of primary tumor	right parietal	right parieto-occipital	splenium of corpus callosum and left parietal	right occipital	left temporal	right fronto-parietal	left frontal
Site of recurrence	right occipital	right parieto-occipital	splenium of corpus callosum and left parietal	genu of corpus collosum and bifrontal	left temporal	right fronto-parietal	left parietal
MRI pre-CTL	08/03/2006	15/01/2009	23/03/2011	15/02/2012	09/05/2012	12/09/2012	06/03/2013
MRI post-CTL	18/04/2006	25/02/2009	15/05/2011	12/03/2012	05/06/2012	08/10/2012	26/03/2013
[^{18}F]FDG pre-CTL	09/03/2006	14/01/2009	23/03/2011	15/02/2012	10/05/2012	14/09/2012	08/03/2013
[^{18}F]FDG post-CTL	N/A	N/A	16/05/2011	17/03/2012	06/06/2012	08/10/2012	27/03/2013
[^{18}F]FHBG pre-CTL	N/A	05/01/2009	21/04/2011	17/02/2012	11/05/2012	13/09/2012	07/03/2013
[^{18}F]FHBG post-CTL	17/04/2006	23/02/2009	09/05/2011	06/03/2012	01/06/2012	04/10/2012	28/03/2013
Lesion total activity pre-CTL	-	10.1	3.5	2.9	23.1	4.1	1.8
Lesion total activity post-CTL	#1, 4.9; #2, 0.8	20.3	8.4	6.3	28.1	8.4	6.8
Non-injected foci total activity pre-CTL	-	-	-	2.4	-	-	1.6
Non-injected foci total activity post-CTL	-	-	-	3.2	-	-	2.7